well as with studies of returned samples and surface magnetic fields is that basin and crater ejecta deposits are major sources of the orbital anomalies. The level of magnetization is weak peripheral to the impact region inside the crater, but it rises beyond the rim and may rise sharply in the case of some ejected materials transported ballistically to large distances. As the latter are probably also the materials most strongly shocked and heated by the impact event, a relative increase in the volume fraction of free iron grains capable of retaining a strong and stable magnetic remanence is to be expected (*1*).

L. L. HOOD
P. J. COLEMAN, JR.
Institute of Geophysics and Planetary Physics, University of California, Los Angeles 90024
D. E. WILHELMS
U.S. Geological Survey, Menlo Park, California 94025

References and Notes

1. D. Strangway, W. Gose, G. Pearce, J. Carnes, in *Magnetism and Magnetic Materials—1972*, C. Graham, Jr., and J. Rhyne, Eds. (American Institute of Phsics, New York, 1973), pp. 1178–1196; M. Fuller, *Rev. Geophys. Space Phys.* **12**, 23 (1974); P. Dyal, C. Parkin, W. Daily, *ibid.*, p. 568.
2. P. Coleman, Jr., and C. Russell, *Philos. Trans. R. Soc. London Ser. A* **285**, 489 (1977); C. Russell, P. Coleman, Jr., B. Fleming, L. Hilburn, G. Ioannidis, B. Lichtenstein, G. Schubert, *Proc. 6th Lunar Sci. Conf.* (1975), pp. 2955–2969; C. Russell, P. Coleman, Jr., G. Schubert, *Science* **186**, 825 (1974).
3. L. Hood, C. Russell, P. Coleman, Jr., *Proc. 9th Lunar Planet. Sci. Conf.* (1978), pp. 3057–3078.
4. P. Coleman, Jr., B. Lichtenstein, C. Russell, L. Sharp, G. Schubert, *Proc. 3rd Lunar Sci. Conf.* (1972), pp. 2271–2286; P. Coleman, Jr., C. Russell, L. Sharp, G. Schubert, *Phys. Earth Planet. Inter.* **6**, 167 (1972); P. Coleman, Jr., G. Schubert, C. Russell, L. Sharp, *NASA Spec. Publ. SP-289* (1971); *Moon* **4**, 419 (1972).
5. L. Srnka, *Proc. 8th Lunar Sci. Conf.* (1977), pp. 785–792.
6. S. K. Runcorn, *Phys. Earth Planet. Inter.* **10**, 327 (1975).
7. R. Lin, *Lunar and Planetary Science IX* (Lunar and Planetary Institute, Houston, 1978), pp. 651–653.
8. D. Strangway, W. Gose, G. Pearce, R. McConnell, *Nature (London)* **246**, 112 (1973).
9. R. Regan, *Geophys. Rev.*, in press.
10. The Fra Mauro Formation is a roughly textured blanket of debris deposited at the time of the Imbrium impact. The Cayley Formation is a smooth light plains unit found all around the moon but concentrated on the southern and southeastern periphery of the Fra Mauro Formation. It is believed to represent either direct deposition of ballistically transported ejecta from the Imbrium and Orientale events or indirect deposition of local materials due to secondary cratering at the time of these events. (*16*, pp. 37–39).
11. Assuming an (altitude)$^{-2.5}$ dependence as a first approximation indicates that the Reiner γ anomaly is the largest in absolute terms as well across the near side within the region of coverage. A number of farside anomalies, including those near the craters Van de Graaff and Aitken, appear to be as much as three to five times larger than the Reiner γ anomaly when scaled to a common altitude.
12. J. McCauley, *U.S. Geol. Surv. Map I-491* (1967).
13. According to D. W. G. Arthur (personal communication), mare ridges similar to those transecting the Reiner γ deposit have slopes 20 to 50 m high where they have been measured in other areas. The ridges that transect the deposit cast shadows on available telescopic photos (taken at low sun illumination angles) that show no shadows for the deposit itself. Additional visual searches (which have higher resolving power than photos under good conditions) also showed no shadows for the deposit. On this basis, a maximum *mean* thickness of 10 m is estimated.
14. M. Talwani, *Geophysics* **30**, 797 (1965).
15. The mean of the radial component for orbits 238, 240, and 242 (Fig. 1) was used to represent the maximum radial component amplitude of the anomaly. The error estimate is a reflection of the standard deviation from the mean for these three measurements.
16. S. R. Taylor, *Lunar Science: A Post-Apollo View* (Pergamon, New York, 1975), pp. 276–279.
17. L. Soderblom and L. Lebofsky, *J. Geophys. Res.* **77**, 279 (1972); L. Soderblom and J. Boyce, *NASA Spec. Publ. SP-315* (1972), pp. 29:3–29:6; J. Boyce and A. Dial, Jr., *Proc. 6th Lunar Sci. Conf.* (1975), pp. 2585–2595.
18. J. Boyce, *Proc. 7th Lunar Sci. Conf.* (1976), pp. 2717–2728. No samples were returned from western Oceanus Procellarum.
19. P. Schultz, *Moon Morphology* (Univ. of Texas Press, Austin, 1976), pp. 420–423.
20. V. Oberbeck and R. Morrison, *Moon* **9**, 415 (1974).
21. F. El-Baz, *NASA Spec. Publ. SP-315* (1972), pp. 29:93–29:97.
22. D. Wilhelms and F. El-Baz, *U.S. Geol. Surv. Map I-948* (1977).
23. Frontispiece, *Proc. 8th Lunar Sci. Conf.* (1977).
24. D. Stuart-Alexander, *U.S. Geol. Surv. Map I-1047* (1978).
25. P. Schultz and D. Gault, *Moon* **12**, 159 (1974).
26. H. Moore, C. Hodges, D. Scott, *Proc. 5th Lunar Sci. Conf.* (1974), pp. 71–100.
27. We thank C. T. Russell and H. Weiss for numerous helpful and informative discussions. Supported by NASA grant NGR-05-007-351.

5 December 1978

Fluidization: Hydrodynamic Stabilization with a Magnetic Field

Abstract. *Fluidization of magnetizable particles by a gas stream in the presence of a uniform applied magnetic field oriented parallel to the flow prevents the hydrodynamic instability that otherwise leads to bubbles and turbulent motion within the medium. The fluidized emulsion expands uniformly in response to gas flow speeds in excess of that at the incipient fluidization point, with transition from the quiescent stable state to bubbling occurring suddenly at a characteristic increased rate of flow. Experimental data demonstrate the dependence of this transition velocity on the intensity of the applied magnetic field, length of the bed, and type of magnetic solids. Data illustrate the pressure distribution through the bed medium, the bed flow characteristics, and other related phenomena.*

This report describes magnetic stabilization of the uniform flow of gas relative to fluidized solids under conditions where gas bubbles normally appear. Fluidized beds first became of major importance through the development of a fluidized process for cracking heavy hydrocarbon into petroleum naphtha (*1*), and many applications in fossil fuel conversion and other areas are foreseen.

The phenomenon of fluidization can be visualized in terms of the simple experiment depicted in Fig. 1A, where a bed of solid particles is supported on a horizontal porous grid in a vertical tube. Gas or liquid is forced to flow upward through this grid and so through the particle bed. The flow causes a pressure drop across the bed, and when the pressure drop is sufficient to support the weight of the particles, the bed is said to be incipiently fluidized. The fluidized bed thus formed has many of the properties of a liquid: objects float on the surface, and the addition or withdrawal of solid particles in process equipment is also facilitated (*2*).

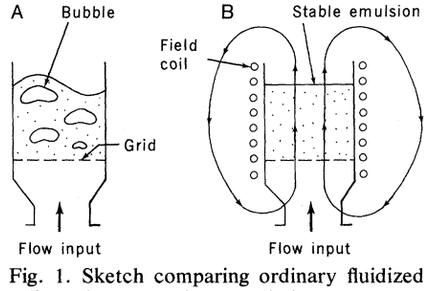

Fig. 1. Sketch comparing ordinary fluidized solids with magnetically stabilized ones. (A) Generally accepted bubbling model for fluidized beds pictures local flow velocities and fraction voids in the dense phase as essentially those of a bed at minimum fluidization; excess flow passes through the bed in the form of bubbles. (B) Magnetically stabilized fluidized solids are free of bubbles; the stabilized emulsion expands homogeneously to accommodate throughflow in excess of minimum fluidization. An applied field that is uniform and colinear with the flow produces the widest range of stabilized operation.

For a gas-fluidized bed in which the gas velocity is greater than the incipient gas velocity, most of the excess gas passes through the bed as bubbles. The bubbles agitate the bed in passing through and promote heat transfer, but some of the gas in the bubbles bypasses the particles altogether, lowering the efficiency of contacting. In addition, the bubbles promote attrition and entrainment of solids, bed slugging (*3*), and uncertainties in process scale-up (*4*).

By providing the solids of the bed with magnetizability and applying a uniform magnetic field that is steady in time and oriented parallel to the direction of gas flow (Fig. 1B), I found that bubble-free fluidized beds are obtained over a substantial range of gas velocities. These

0036-8075/79/0406-0057$00.50/0

stabilized beds do not have the relatively high heat transfer rates of bubbling fluidized beds, but the backmixing of solids and gas bypassing that are characteristic of conventional beds are eliminated (*5*). The magnetic field may be conveniently furnished by wound coils carrying a modest electric current and surrounding the fluidization vessel (*6*). Experiments showing certain general characteristics of the magnetically stabilized solids are described below.

Figure 2A illustrates the response of magnetized solids to an increase of the superficial velocity of the gas for a constant applied magnetic field. The particles are a closely graded range of ferromagnetically soft nickel-copper alloy particles (Monel) (*7*). With no gas flow, the bed length is that of the randomly dumped solids. With a flow of air admitted to the vessel, the bed length is unchanged up to the point of incipient fluidization. Thereafter, the bed accommodates increasing flow by a process of homogeneous expansion in which bubbles are absent from the bed and the bed emulsion is free of agitation or solids circulation. In this state a visual inspection of the static bed fails to reveal its fluid-like nature. However, objects are readily immersed in the bed as in a liquid, and when released, light objects float and dense objects sink. When a hollow plastic sphere (Ping-Pong ball) 3.72 cm in diameter and weighing 1.94 g is initially rotated in the bed, it continues to spin for several seconds, indicating the very low frictional support it experiences when floating partly submerged in the bed emulsion. As the gas flow rate is increased further, a point is ultimately reached where bubbling and fluctuation in pressure drop suddenly begin (*8*). As detailed in Fig. 2A, this point of transition from the calmed or stabilized state of flow to the state of bubbling and turbulence occurs at a flow rate substantially higher than that at incipient fluidization. Additional study showed that the transition velocity of a stabilized bed was unaffected by the cross section dimensions of the containing vessel in tests where the hydraulic diameter varied from 3 to 28 cm.

Transition velocity increases as bed length decreases, and for long beds it appears that transition speed asymptotically approaches a constant value. The behavior of Monel particulates of three size ranges is shown in Fig. 2B; transition speed is highest for the largest particles, all other variables held constant. The increased stability of shorter beds may be explained by considering the evolution of a small hydrodynamic disturbance introduced at the grid. The disturbance grows as it moves through the bed, but may be sped out of the bed before it grows sufficiently to produce a bubble.

Other magnetizable solids behave similarly. Experimental results with steel spheres (Fig. 2, C and D) illustrate further aspects of the behavior. Figure 2C shows that measurement of the pressure difference through the bed as a function of flow rate gives a curve that rises linearly from the origin, breaks at the point of incipient fluidization, and then levels off; the pressure drop is then nearly equal to the weight of the bed divided by its cross-sectional area. The slope of the initial linear portion of the curve is independent of applied field and is predictable from the low-velocity limit of the well-known fixed-bed Ergun relationship (*4*, p. 67). When the test is conducted with another value of applied magnetic field, the initial slope and plateau value

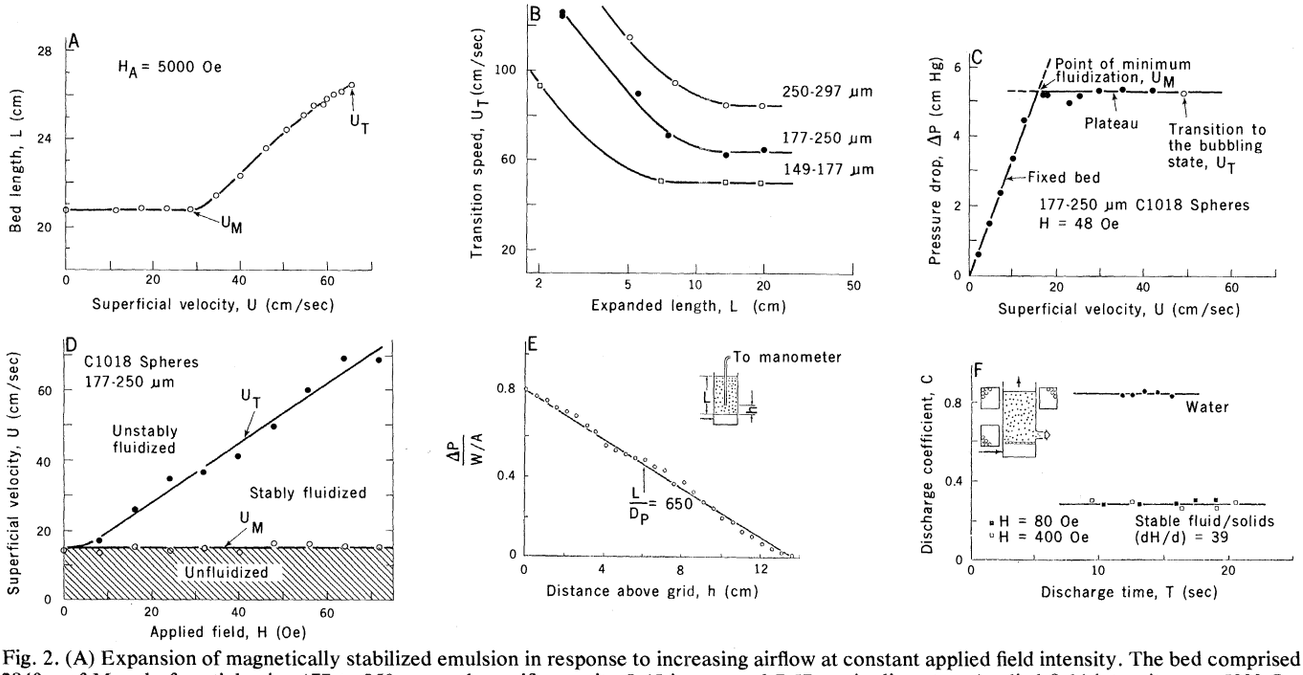

Fig. 2. (A) Expansion of magnetically stabilized emulsion in response to increasing airflow at constant applied field intensity. The bed comprised 2840 g of Monel of particle size 177 to 250 μm and specific gravity 8.45 in a vessel 7.57 cm in diameter. Applied field intensity was 5000 Oe, uniform over the test region to within 1 percent. (B) Influence of bed length on transition speed for magnetically saturated beds of Monel particulates in applied field of 5000 Oe. Plateau values of transition speed define beds that are long. (C) Characteristic breakpoint and plateau. Bed particles were 177 to 250-μm C1018 steel spheres. Pressure was sensed by a capillary tube insert vertically into the bed with the tip about 1 mm above the bed support grid and the other end connected to a U-tube manometer. Reduction of flow rate after reaching any plateau point in the stabilized region is accompanied by decrease of pressure approximately linearly back through the origin, and further cycling produces a hysteresis loop. In these modes of operation the bed is partially levitated. (D) Transition from the unfluidized to stably fluidized and then to unstably fluidized (bubbling) state as a function of applied field for steel spheres in (C). In the stably fluidized state the medium exhibits liquid-like behavior of buoyancy and flow. At values of H higher than those shown here the stably fluidized medium develops properties of a gel, then at higher field becomes solid. (E) Gauge pressure versus depth in bed. Constant slope indicates uniform voidage from layer to layer [$\epsilon_0 = 1 - (\partial \Delta p/\partial l)/\rho_s g$]. The solids were nickel supported on alumina. (F) Flowable nature of magnetized, fluidized solids demonstrated in orifice discharge tests. Discharge coefficient was calculated as described in (*12*). Bed solids were nickel on alumina, 250 to 420 μm.

are unchanged. This behavior is the same as for unmagnetized, fluidized solids. The invariance of incipient fluidization to the presence or absence of the applied field is anticipated since a uniform field can exert no net force on a whole body.

In Fig. 2C the breakpoint corresponds to the minimum fluidization speed u_M, and transition to the bubbling state of flow at speed u_T corresponds to the onset of fluctuations in pressure and to visible bubbling at the bed top surface. At speeds in excess of u_T the bed contains bubbles throughout and bed length fluctuates widely.

When pressure-drop flow-rate curves are obtained for a number of applied field intensities, the values of u_M and u_T plotted against applied field H produce the map shown as Fig. 2D. This defines three regions that classify the physical state of the bed emulsion as unfluidized, stably fluidized, or unstably fluidized. The boundary between stably and unstably fluidized represents the transition described previously, while the boundary between unfluidized and stably fluidized represents incipient fluidization. The horizontal line through the values of u_M shows that incipient fluidization is unaffected by the applied field intensity.

Uniformity of the emulsion can be inferred from pressure measurements made with a capillary tube connected to a manometer and inserted vertically into the bed. Pressure increases linearly with depth, implying that voidage is uniform from one layer to the next throughout the bed (Fig. 2E).

Orientation of the applied field is an important parameter in achieving the maximum range of stable flow; the preferred direction is colinear or parallel to the direction of flow, and hence vertical in these experiments. Experiments with a uniform transverse orientation of the applied field showed that bubbling occurs at a flow rate that is greater than the incipient fluidization velocity, but much less than the transition velocity for a colinear field of the same intensity (*9*).

Orifice discharge tests confirmed the ability to transfer solids out of the containing vessel. The flow rate of the solids is characterized by a constant value of the discharge coefficient, independent of the applied field intensity or initial depth of the bed (Fig. 2F). Water is discharged with a larger coefficient, presumably because of arching that impedes the flow of grains through orifices when the ratio of orifice diameter to particle size is too small. Additional tests in which bands of surface-pigmented solids were used as a color tracer showed that solids move

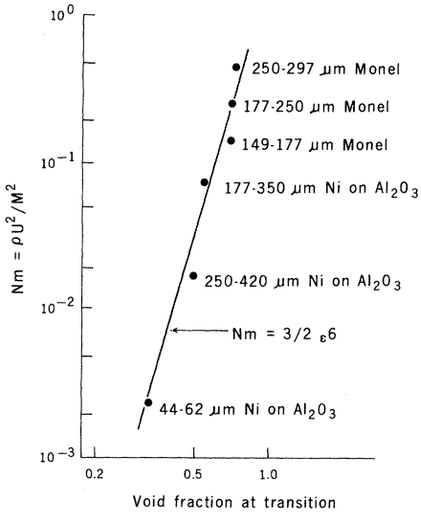

Fig. 3. Correlation of transition speed with void fraction. Bed particulates are magnetically saturated, and bed is asymptotically long (horizontal portion of curves in Fig. 2A).

through the bed in ideal piston-like motion with no backmixing when a series of eight evenly spaced orifices are simultaneously opened around a circumference of the vessel's cylindrical wall a short distance above the support grid. The plug nature of the flow is participated in by all the bed particles, including those adjacent to the wall. In this respect, the bed emulsion behaves as an inviscid medium displaying slip at the wall. Of course, near the orifices the flow must deviate from simple one-dimensional motion.

When particle magnetization exceeds a threshold value dependent on the particulars of the flow test, the flowability of the bed solids is impeded and ultimately lost because of particle-to-particle forces of cohesion.

In seeking a universal description of the magnetic transition phenomenon, analytical model study as well as dimensional reasoning led to the conclusion that for a long bed of magnetically saturated solids fluidized by a gas of negligible density the transition speed U (centimeters per second), particle density ρ (grams per cubic centimeter), magnetization M (gauss), and bed voidage ϵ are functionally related through (*10*)

$$N_m = f(\epsilon)$$

Here N_m is a dimensionless magnetic modulus representing a ratio of kinetic energy to magnetostatic field energy and defined by

$$N_m = \frac{\rho U^2}{M^2}$$

Limited data for media of 335-μm Monel, 335-μm supported nickel, and 53-μm supported nickel in which voidage varies from 0.35 to 0.77 and N_m varies from 2.6×10^{-3} to 0.30 are correlated as shown in Fig. 3 by

$$N_m = \frac{3}{2}\epsilon^6$$

Magnetically stabilized fluidized media provide a unique new means for the contacting of fluids with solids, offering an alternative to conventional fluidized beds, fixed beds, moving beds, and other types of contactors (*11*). Since gas bypassing and solids backmixing are prevented and solids flow is accommodated, stabilization offers the capability for true countercurrent contacting in continuous flow systems. Fine particle sizes can be used that are especially suited for catalytic conversions, sorption separations, and other operations without penalties of a high pressure drop. The gentle nature of the solids flow permits the use of friable materials and minimizes losses of these solids. Potential applications are in petroleum refining, coal gasification, ore roasting, flue gas treatment, and other areas.

It was also found that the bed functions as an effective filter to remove contaminant particulates from a gas stream. The efficiency for collection of fly ash in a 10-cm-long stabilized filter bed of 250- to 420-μm magnetite particles as measured by an Anderson impactor in preliminary tests was 99.9 percent or greater for particulates of 4 μm and larger, and 95 percent for particulates of 2.1 μm. The applied field was 150 Oe with a superficial velocity of 60 cm/sec. The process is promising for particulate collection at elevated temperatures and pressures beyond the state of the art for electrostatic precipitators and other collecting devices; operation is conceivable up to the vicinity of the Curie temperature (1121°C for elemental cobalt). Since the bed is fluidized, the bed contents may be removed for cleaning on a continuous basis and the pressure drop remains nearly constant in operation, even when several weight percent of fines has been collected.

RONALD E. ROSENSWEIG
Corporate Research Laboratories, Exxon Research and Engineering Company, Linden, New Jersey 07036

References and Notes

1. Fundamental experiments in fluidization and transport of solids were carried out at Massachusetts Institute of Technology by W. K. Lewis and E. R. Gilliland in the early 1940's (*4*, p. 19). Plant scale development is described by E. V. Murphree, C. L. Brown, H. G. M. Fischer, E. J. Gohr, and W. J. Sweeney [*Ind. Eng. Chem.* **35**, 768 (1943)].
2. J. F. Davidson and D. Harrison, *Fluidized Particles* (Cambridge Univ. Press, Cambridge, England, 1963).

3. J. M. Matsen and B. L. Tarmy, *Chem. Eng. Prog. Symp. Ser. No. 101* (1970), p. 1.
4. D. Kunii and D. Levenspiel [*Fluidization Engineering* (Wiley, New York, 1969)] discuss failure of the scale-up of a hydrocarbon synthesis plant and other problems.
5. This is related to the behavior of magnetic stress in the medium, considered as a homogeneous magnetized continuum. A local perturbation in voidage modifies the uniform stress of the unperturbed bed, creating forces that restore the medium to the uniform state (R. E. Rosensweig, *Ind. Eng. Chem. Fundam.*, in press). For a treatment of the hydrodynamics of the growth of perturbations in conventional fluidized solids see T. B. Anderson and R. Jackson [*ibid.* **7**, (No. 1), 12 (1968)].
6. Previous investigators have apparently overlooked the sufficient role played by orientation and uniformity of the applied magnetic field [for example, D. G. Ivanov and G. T. Grozev, *C. R. Acad. Bulg. Sci.* **23** (No. 7) 787 (1970); and R. L. Sonoliker *et al.*, *Ind. J. Technol.* **10**, 377 (1972)]. In a uniform applied magnetic field the bed is free of any magnetic force, but previous workers have often attributed the delay of bubbling at higher flow rates to a magnetic force added to the force at gravity. More important as a distinguishing feature is the existence of the stabilized, levitated range reported here at velocities between μ_M and μ_T [R. E. Rosensweig, U.S. Patent No. 4,115,927 (1978)].
7. Measurements of a particulate sample with a vibrating sample magnetometer gave magnetization values of 372 G at an applied field of 5000 Oe, 326 G at 3000 Oe, 250 G at 1000 Oe, and 132 G at 200 Oe. The material is ferromagnetically soft with a remanence of less than 5 G.
8. As the flow rate of the gas is slowly increased to the vicinity of the transition point, the bed surface in some instances bubbles over part or all of its area for a limited time, then returns to the motionless state; apparently the medium adjusts to a new structure. An incremental increase in throughput then produces steady bubbling and is taken as the experimental transition point.
9. Particles comprising nickel supported on alumina that were crushed and sieved to the size range 0.177 to 0.250 mm formed a bed with a settled height after aeration of 14 mm. In the absence of applied magnetic field, surface bubbling occurred at a superficial velocity of 2.9 cm/sec. With application of a transverse magnetic field of 570 Oe, transition to bubbling was increased somewhat to 4.3 cm/sec. In an axially oriented field of 570 Oe the bed expanded quiescently to 20.0 cm/sec, where momentary bubbling occurred (transition with restructuring), followed by quiescent expansion to 29.0 cm/sec, where transition to steady bubbling was observed.
10. For the long, magnetically saturated beds U depends only on ρ, M, ϵ, g, and F where g is the gravitational constant and F is the fluid-particle drag force per unit volume of the emulsion. Dimensional reasoning simplifies the relationship to the interdependence among the three groups, $\rho U^2/M^2$, ϵ, and $F/\rho g$. The condition of fluidization is $(F/\rho g) = 1 - \epsilon$, so that $\rho U^2/M^2$ is uniquely related to the ϵ alone.
11. Experiments with electrofluidized beds are reported by T. W. Johnson and J. R. Melcher [*Ind. Eng. Chem. Fundam.* **14**, 146 (1975)], P. W. Dietz and J. R. Melcher [*ibid.* **17**, 112 (1978)], G. M. Colver [*Powder Technol.* **17**, 9 (1977)], and others. There should be parallels to the magnetic stabilization, although these investigators focused on particulate collection in turbulent beds and the influence of the electric field on bubble dynamics. There seems to be no indication that electrically calmed beds are flowable. Polarization forces developed in electric fields are not as strong as those that can be developed in magnetic fields, while the existence of free charge in such beds has no analog in the magnetic case.
12. Discharge coefficient was calculated from

$$C = \frac{L^{1/2} - L_o^{1/2}}{(g/2)^{1/2}} \frac{1}{T} \left(\frac{d_b}{d_o}\right)^2$$

where L is initial depth over orifice center, L_0 the depth after time T, d_b the bed diameter, d_o orifice diameter, and g the gravitational constant (980 cm/sec^2). For the system in Fig. 2F, L is 8 to 14 cm, and L_0 is 4 cm; d_b is 7.37 cm (inner diameter), d_o = 0.83 cm, and gas superficial velocity, 15.6 cm/sec.
13. I thank J. J. Schlaer for his invaluable help in carrying out the experiments.

18 September 1978; revised 4 December 1978

Interplanetary Magnetic Field Polarity and the Size of Low-Pressure Troughs Near 180°W Longitude

Abstract. *When the interplanetary magnetic field is directed away from the sun, the area of wintertime low-pressure (300-millibar) troughs near 180°W longitude is significantly larger than when the field is toward the sun. This relation persists during most of the winters of 1951 to 1973.*

Low-pressure (300-mbar) troughs (cyclones) that are near 180°W longitude when the interplanetary magnetic field is directed away from the sun are, on the average, significantly larger than when the field is toward the sun. The difference in area persists during a 5-day interval in which the troughs move from 180°W to the North American continent. This relation persists during most of the winters from 1951 to 1973. (The winter of 1951 is defined as October 1950 through March 1951.)

Roberts and Olson (*1*) reported that troughs that cross 180°W 2 to 4 days after an increase in geomagnetic activity tend to become significantly larger than average. The size of the troughs was measured by using the vorticity area index (VAI), which is defined as the area of the trough where the absolute vorticity (circulation per unit area) at 300 mbar exceeds a value of 20×10^{-5} sec^{-1} plus the area where the vorticity exceeds 24×10^{5} sec^{-1}. These vorticity values correspond to a well-formed trough. The VAI was recorded for a trough on the first day after it had crossed 180°W during the course of its eastward motion (occasionally a trough was formed east of 180°W and was similarly counted). After a trough had been identified east of 180°W, its VAI was measured twice a day for the next 12 days (during some winters the area was recorded for only the first 3 days and during some early years data were available only once a day). In the study reported here we used the same measurements of trough area that were used by Roberts and Olson (*1*); however, in the present study there is no reference to the times of sector boundary passages (and therefore to times of varying geomagnetic activity), so the results reported here are not directly comparable to those of Roberts and Olson. In some of our earlier work (*2*) the VAI summed over all troughs in the entire

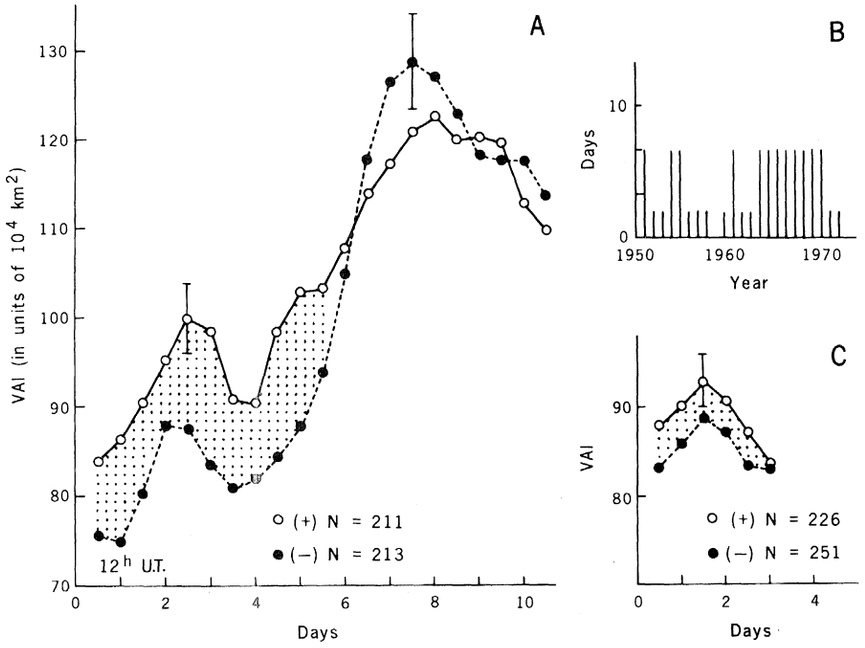

Fig. 1. (A) Average area of low-pressure troughs (cyclones) during the 10 days after the troughs crossed 180°W: (○) away troughs and (●) toward troughs (see text for explanation). During the first 5 days after the troughs crossed 180°W, the area of the away troughs is significantly larger than the area of the toward troughs. Error bars are plus or minus the standard error of the mean. (B) Indication of winters during which trough area data were available for 10 days after the troughs crossed 180°W and of winters during which the data were available for only 3 days. (C) Same as first 3 days in (A) but computed for years in which trough area data were available for only 3 days. The area of the away troughs is again larger than the area of the toward troughs.

0036-8075/79/0406-0060$00.50/0